Magnetic ground state of the frustrated honeycomb lattice antiferromagnet $Bi_3Mn_4O_{12}(NO_3)$

N. Onishi,[1] K. Oka,[1,2] M. Azuma,[1,2,*] Y. Shimakawa,[1] Y. Motome,[3] T. Taniguchi,[4] M. Hiraishi,[5] M. Miyazaki,[5] T. Masuda,[6] A. Koda,[5,6] K. M. Kojima,[5,6] and R. Kadono[5,6]

[1]*Institute for Chemical Research, Kyoto University, Uji, Kyoto 611-0011, Japan*

[2]*Materials and Structures Laboratory, Tokyo Institute of Technology, 4259 Nagatsuta, Midori-ku, Yokohama 226-8053, Japan*

[3]*Department of Applied Physics, University of Tokyo, Tokyo 113-8656, Japan*

[4]*Graduate School of Science, Osaka University, Osaka, Toyonaka 560-0043, Japan*

[5]*Department of Materials Structure Science, The Graduate University for Advanced Studies, Tsukuba, Ibaraki 305-0801, Japan*

[6]*Muon Science Laboratory and Condensed Matter Research Center, Institute of Materials Structure Science, High Energy Accelerator Research Organization (KEK), Tsukuba, Ibaraki 305-0801, Japan*

(Received 28 June 2011; revised manuscript received 29 February 2012; published 11 May 2012)

$Bi_3Mn_4O_{12}(NO_3)$, in which the Mn^{4+} ions carry $S = 3/2$, is the first honeycomb lattice system that shows no long-range magnetic ordering. We investigated the magnetic ground state of this compound by measuring magnetic susceptibility and μSR with a pure powder sample synthesized under an improved reaction condition. It was found that the system underwent a spin glass transition at 6 K in a zero magnetic field. A comparison of the temperature dependence of the magnetic susceptibility with the results of a Monte Carlo simulation suggests the importance of intra-bilayer coupling and further neighbor interactions beyond those of second neighbors.

DOI: 10.1103/PhysRevB.85.184412 PACS number(s): 75.10.Jm, 75.50.Ee, 75.40.Mg, 76.75.+i

I. INTRODUCTION

Triangular and kagome antiferromagnets attract much attention because of the presence of geometrical magnetic frustration.[1–5] Like a kagome lattice, the honeycomb lattice is a derivative of the triangular lattice and is obtained by periodically removing 1/3 of the spins from a triangular lattice. Since an ideal antiferromagnetic (AF) honeycomb system with only the AF nearest-neighbor interaction (J_1) is free from frustration, the ground state is long-range ordering. However, the system becomes frustrated if the next-nearest interaction (J_2) is also AF, as shown in Fig. 1(a). According to theoretical calculations, a honeycomb antiferromagnet does not show long-range ordering when $J_2/J_1 > 1/6$ (for classical spin)[6] or > 0.15 (for $S = 3/2$).[7]

$Bi_3Mn_4O_{12}(NO_3)$ consists of $S = 3/2$ antiferromagnetic honeycomb lattices.[8] Edge-sharing MnO_6 octahedra form undistorted honeycomb lattices that are separated by Bi^{3+} and NO^{3-} layers. The threefold symmetry of the NO^{3-} layers acts as a template to form regular honeycomb layers, as shown in Fig. 1(b). It should be pointed out that NO^{3-} layers are inserted periodically, leading to alternating short (4.78 Å) and long (8.38 Å) honeycomb interlayer distances. This compound can therefore be regarded as a bilayer system. No long-range AF ordering was found at temperatures as low as 0.4 K, despite a relatively large Weiss constant of -257 K.[8] Accordingly, it is suggested that $Bi_3Mn_4O_{12}(NO_3)$ is a geometrically frustrated system. Since J_1 mediated by Mn-O-Mn bonds at an angle of approximately 100° is rather weak, J_2 mediated by the Mn-O-O-Mn bond can be competitive. The possible geometrical frustration in $Bi_3Mn_4O_{12}(NO_3)$ promoted theoretical investigations,[9–11] but no estimation of antiferromagnetic interactions on the basis of an analysis of magnetic susceptibility has been made because of the presence of magnetic impurity, MnO_2, which influenced the susceptibility data. Magnetization and neutron powder diffraction studies revealed the presence of a peculiar magnetic-field–induced long-range ordering at around 6 T and 10 K in this system.[12,13] However, the ground state in zero magnetic field is unclear.

In this report, we investigated the magnetic ground state of $Bi_3Mn_4O_{12}(NO_3)$ by measuring direct current (DC) and alternating current (AC) susceptibility, specific heat, and μSR[14] with a pure powder sample synthesized under an improved reaction condition. It was revealed that the system underwent a spin glass transition at 6 K in a zero magnetic field. The magnitude of J_1 and the ratio of J_2 to J_1 were estimated by comparing the experimental susceptibility and a Monte Carlo simulation.

II. EXPERIMENT

The sample powder was prepared by mixing $Mn(NO_3)_2{\cdot}6H_2O$ and $NaBiO_3$ (Wako) in a molar ratio of 8.99 to 1.00 by hydrothermal reaction between 513 and 553 K for 3 to 7 days in a 70-mL Teflon-lined autoclave. A possible reaction process is $3NaBiO_3 + 4Mn(NO_3)_2 + 2H_2O \rightarrow Bi_3Mn_4O_{12}(NO_3) + 3NaNO_3 + 4HNO_2 + 1.5O_2$. Only $Bi_3Mn_4O_{12}(NO_3)$ crystallized, and $NaNO_3$ and HNO_3 remained in the solution. A synchrotron X-ray powder diffraction (SXRD) measurement was performed by using the beamline BL02B2 at the SPring-8 facility. The data were collected at a constant wavelength ($\lambda = 0.778$ Å) at room temperature.

The DC magnetic susceptibility was measured with a SQUID magnetometer (Quantum Design MPMS XL) during heating after zero-field cooling (ZFC) and during cooling between 2 and 400 K in a magnetic field of 0.1 T. The specific heat of a solidified pellet was measured at temperatures between 2 and 300 K by a relaxation method using a Quantum Design Physical Property Measurement System (PPMS). Both the in-phase (χ') and out-of-phase (χ'') components of the AC susceptibility were measured with a SQUID magnetometer (Quantum Design MPMS XL) on heating in an AC field of 4.0 Oe from 1 to 50 K. The data were integrated over 2.17 h at each temperature.

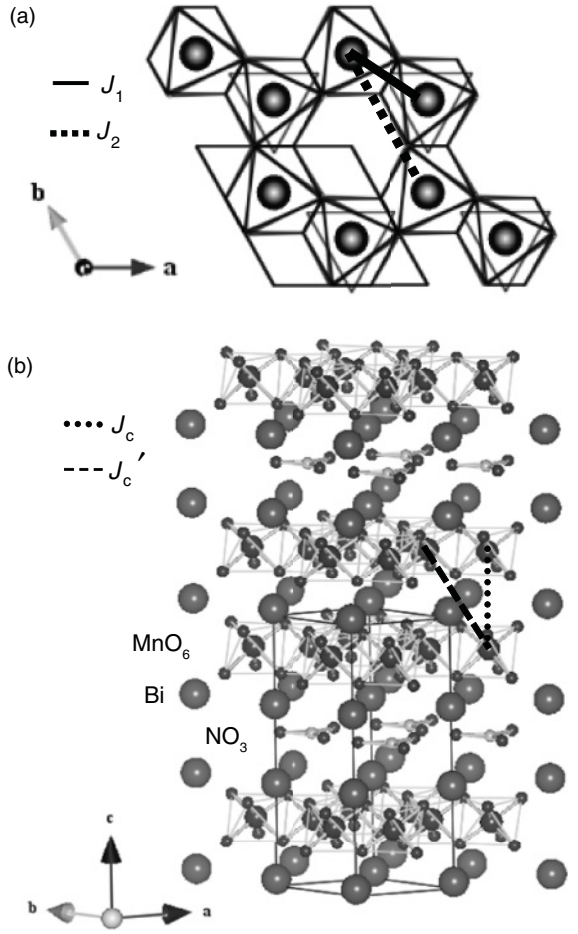

FIG. 1. The Mn-O network in a honeycomb layer (a) and the crystal structure of $Bi_3Mn_4O_{12}(NO_3)$ (b). Solid, dotted, and double lines show the position of the nearest (J_1), the next-nearest neighbor (J_2), and the opposite site (J_3) interactions. The face-to-face (J_c) and the diagonal (J_c') intra-bilayer interactions are also indicated.

The μSR measurements were performed at the D1 area of J-PARC MUSE in Japan and at M20 at TRIUMF in Canada. The μ^+-e^+ decay asymmetry was measured in longitudinal fields up to 0.01 T by cooling down to 2 K.

A Monte Carlo (MC) simulation was performed for a classical spin Heisenberg model on a double-layer honeycomb lattice. We used the exchange MC technique,[15] taking the temperature grid logarithmically for fast convergence at low temperatures. Periodic boundary conditions were employed. We performed 5×10^5 MC samplings typically for measurement after 2×10^4 MC steps for thermalization. In the following, we show the data for a system size with 2304 spins (24×24 unit cells, 2 layers), for which we confirmed that the system size dependence was negligible in the relevant temperature range.

III. RESULTS AND DISCUSSION

A. Sample preparation

The sample preparation condition was examined as follows. From experience, we found Curie-like behavior in magnetic susceptibility at low temperatures, which could be attributed to structural defects were pronounced when the sample was prepared at a low temperature. On the other hand, the amount of by-product MnO_2 increased when the reaction temperature was too high. MnO_2 was produced by the thermal decomposition of $Mn(NO_3)_2{\cdot}6H_2O$ when the amount of water was too small. Consequently, precipitation of MnO_2 was depressed during the reaction by reducing the concentration of the reagents in the reaction solution. The reaction condition was therefore optimized by changing the ratio of reagents to distilled water and by tuning the reaction temperature. The best sample we have ever obtained was synthesized by the hydrothermal reaction of $Mn(NO_3)_2{\cdot}6H_2O$ (9.2 g), $NaBiO_3$ (1.0 g), and distilled water (24 mL) at 543 K for 7 days.

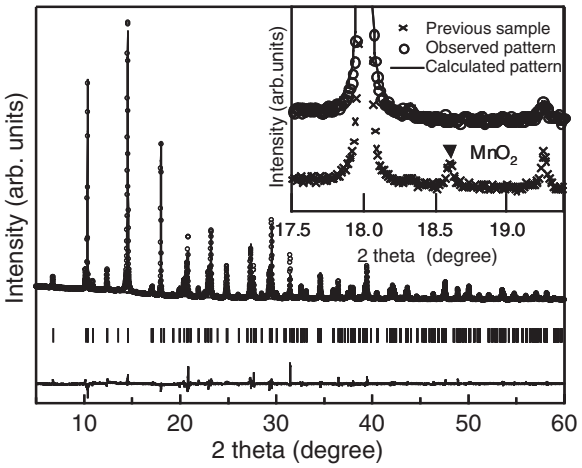

FIG. 2. SXRD pattern of $Bi_3Mn_4O_{12}(NO_3)$ and the Rietveld refinement profile. The observed (dot), calculated (line), and difference (bottom line) patterns are shown. Bragg reflections are indicated by tick marks. Inset shows comparison of the SXRD patterns of the previous and present samples.

Figure 2 shows an SXRD pattern of the sample obtained under the improved reaction conditions. A Rietveld analysis gave satisfactory small reliability factors of $R_{WP} = 3.33\%$ and goodness of fit $= 1.1425$, confirming that the crystal structure of the obtained $Bi_3Mn_4O_{12}(NO_3)$ was the same as in the previous report. As shown in the inset in Fig. 2, the peak derived from the MnO_2 observed for the previous sample was below the background level of 1/300 of the main peak of $Bi_3Mn_4O_{12}(NO_3)$ for the present sample. This therefore proves that $Bi_3Mn_4O_{12}(NO_3)$ without magnetic impurity was obtained.

B. Magnetic susceptibility and specific heat

The temperature dependence of the DC magnetic susceptibility shown in Fig. 3(a) has a broad maximum centered at around 70 K. This broad maximum is a characteristic feature of a low-dimensional antiferromagnet and is consistent with a two-dimensional crystal structure. This feature was well reproduced in the Monte Carlo calculation discussed later. As temperature further decreased, a deviation in the ZFC and field-cooling (FC) data below 9 K and a maximum in the ZFC data at 7 K were observed, suggesting a magnetic transition. There was no corresponding anomaly in the temperature dependence of the specific heat divided by temperature (C_P/T)

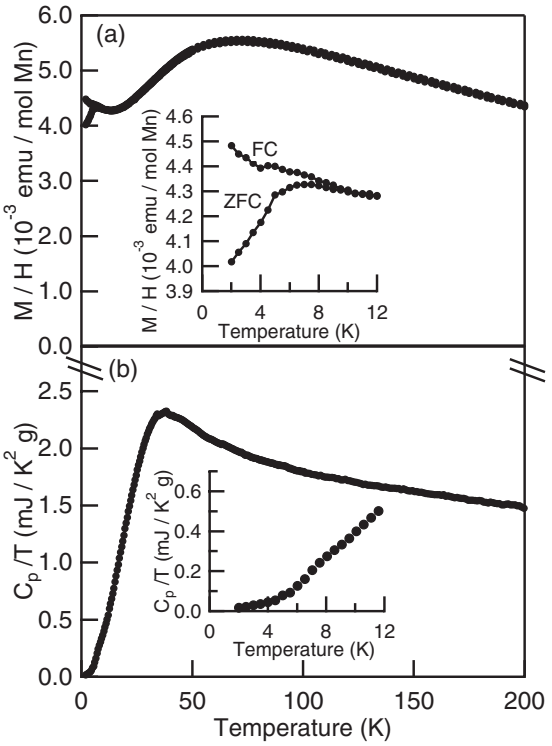

FIG. 3. (a) Temperature dependence of the magnetic susceptibility of $Bi_3Mn_4O_{12}(NO_3)$ in zero field cooling and field cooling conditions. (b) Total specific heat divided by temperature of a solidified $Bi_3Mn_4O_{12}(NO_3)$ pellet. Insets show magnification of the data between 2 K and 12 K.

as shown in Fig. 3(b). Thus, this suggests that the ground state of $Bi_3Mn_4O_{12}(NO_3)$ is not long-range ordering but a spin glass.

For the previous sample, a Curie-like increase in susceptibility was observed below 20 K, which could be attributed to the presence of an undetected impurity phase or to free spins due to structural defects. The present sample scarcely showed such an upturn, suggesting that the number of crystal defects decreased because of the synthesis at a higher temperature. The small peak in the specific heat data at 95 K, owing to the AF ordering of MnO_2 found for the previous sample, was also absent for the present sample. This confirms the absence of MnO_2 impurity, which previously prohibited a detailed analysis of the susceptibility data.

Figure 4 shows the temperature dependence of χ' and χ'' of the AC susceptibility at 1 Hz. Here, χ' shows a cusp at 8 K, in accordance with the DC susceptibility. A maximum in χ'' was also observed at the same temperature, strongly suggesting the spin glass nature. Unfortunately, we could not confirm the frequency dependence of the cusp temperature commonly observed for a spin glass system because the higher-frequency signals were too weak. The absolute value of the magnetic susceptibility at the freezing temperature was close to the sensitivity limit because of the large Weiss temperature and the decrease below the maximum temperature. However, the frequency dependence of the freezing temperature was observed in the neutron diffraction.[12] The broad elastic peak attributed to the short-range ordering increased almost monotonically below the freezing temperature (T_f) measured with the neutron energy scale. T_f strongly depended on the

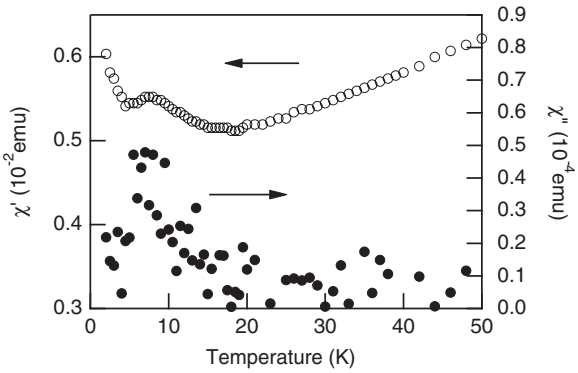

FIG. 4. Temperature dependence of the in-phase (χ') and the out-of-phase (χ'') components of the AC susceptibility at 1 Hz.

energy resolution of the neutrons and became higher due to the broader energy resolution because signals with faster fluctuations were integrated. This temperature and frequency dependence of the fluctuations is the characteristic feature of a spin glass system.

C. μSR measurement

To further investigate the magnetic ground state and determine the freezing temperature, we performed μSR experiments. Figure 5 shows μSR time spectra measured at J-PARC in longitudinal fields up to 0.01 T at 120 K. Muon spin exhibited a slow and Gaussian-like relaxation due to ^{55}Mn nuclear moments. All data can be reproduced well by using the dynamic Kubo–Toyabe function at a fluctuating rate of 0.45(3) μs^{-1}. Seemingly, the observed dynamics were due to the thermal diffusion of muons.[16,17] The obtained dipolar field $B = \Delta/\gamma_\mu = 2.18(6)$ Gauss, where Δ is the dipolar width and γ_μ is the muon gyromagnetic ratio, was in good agreement when a muon was surrounded by six ^{55}Mn ions at a distance of 2.37 Å, strongly suggesting that the muon-stopping site was the center of the Mn hexagon. Positive muons tend to stop at a site showing a local minimum of the electric field potential near negatively charged oxygen ions. However, the observed dipolar field cannot be explained by assuming a muon site is adjacent to one of the MnO_6 octahedra. Furthermore, it is noted that the proposed muon stopping site had high crystallographic

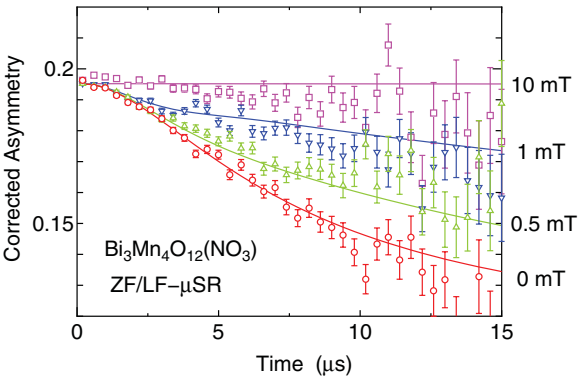

FIG. 5. (Color online) μSR time spectra at 120 K in longitudinal magnetic fields up to 0.01 T. The solid curves represent the result of a fitting analysis by using the dynamic Kubo-Toyabe function.

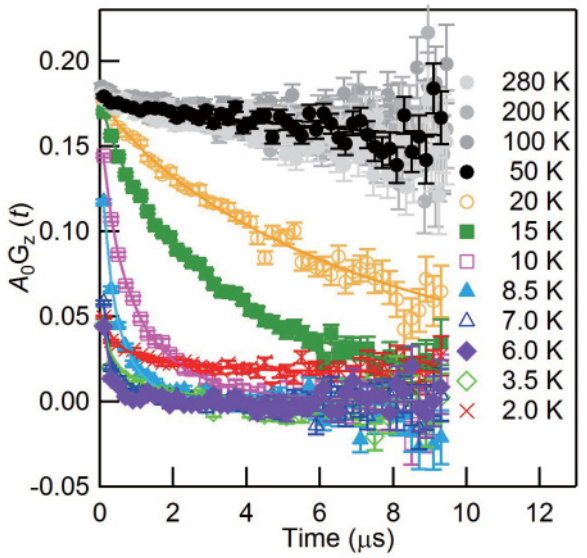

FIG. 6. (Color online) μSR time spectra in a longitudinal field of 0.01 T at various temperatures between 2 to 50 K.

symmetry against both manganese and oxygen ions, having an equal distance between every surrounding oxygen ion.

Figure 6 shows the μSR time spectra obtained at TRIUMF in a longitudinal field of 0.01 T at varying temperatures down to 2 K. No significant difference was observed above 50 K, as seen in Fig. 6. However, fast muon spin relaxation without a precession component in the early time region ($t < 0.1$ μs), which is followed by a slow-relaxing tail ($t > 1$ μs), was observed below 6 K. As seen in Fig. 5, the nuclear magnetic field was entirely decoupled under a field of 0.01 T. Therefore, the observed muon spin relaxation was attributed to electronic spin, suggesting the presence of a random and static internal field, which is characteristic of spin glass. The slow-relaxing part was analyzed by fitting to a single stretched exponential relaxation function $A_0G_z(t) = A_0\exp(-[\lambda t]^{\beta})$. The estimated initial asymmetry A_0, the relaxation rate λ, and the power β are plotted in Fig. 7 as functions of temperature. The sudden decrease of A_0 below 6 K indicates the appearance of an internal magnetic field. Moreover, λ shows a sharp peak at 6 K, indicating that the spin correlation had a singularity at this temperature. These results clearly indicate that the system underwent a magnetic transition at 6 K. This temperature was a bit lower than the cusp temperature of the AC susceptibility, probably because the cusp temperature of the scattered AC susceptibility data was overestimated.

D. Monte Carlo calculation of the magnetic susceptibility

The absence of long-range ordering was therefore confirmed, and the spin glass nature of the ground state was strongly suggested experimentally. Next, we compared the experimental magnetic susceptibility data with the Monte Carlo results in order to estimate the antiferromagnetic interactions. Before the comparison, the experimental data were processed as follows. The data above 300 K were fitted to the Curie-Weiss law $\chi = \chi_0 + C/(T-\theta)$, where $C = N_A g^2 \mu_B^2 S(S+1)$, with $S = 3/2$ and the g value was fixed to 2.00, as determined by an electron spin resonance (ESR) measurement.[18] The fitting

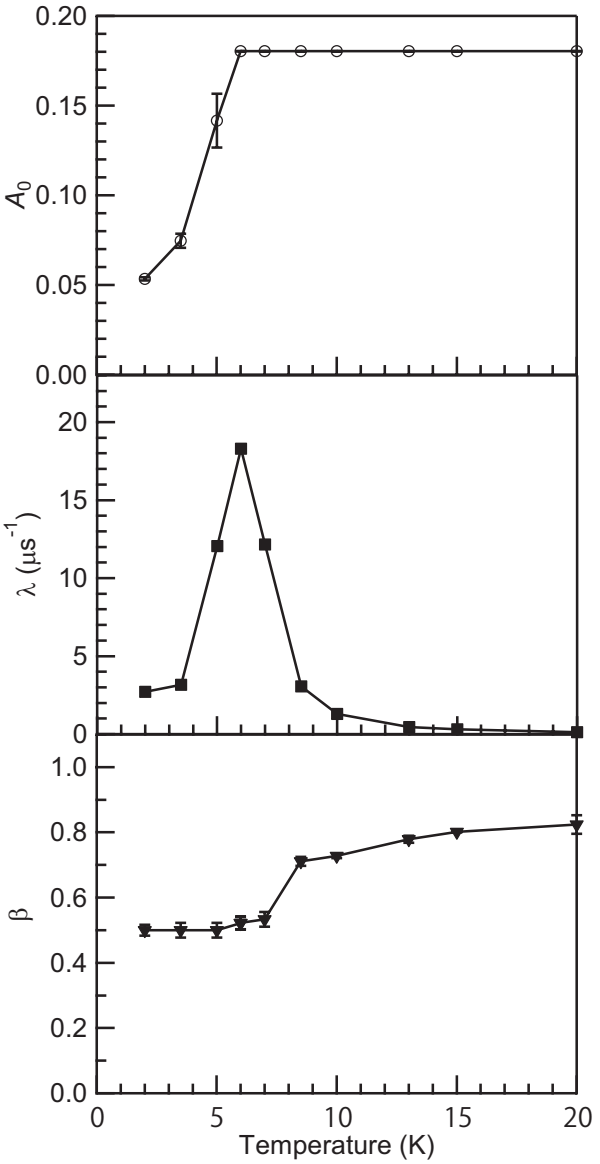

FIG. 7. Temperature dependence of the initial asymmetry (A_0), relaxation rate (λ), and the power (β) in a longitudinal field of 0.01 T.

gave the Weiss constant $\theta = -222$ K and the temperature independent term $\chi_0 = -2.25 \times 10^{-4}$ emu/mol Mn. The obtained χ_0 was subtracted from the experimental data for comparison with the calculations.

First, we tried a single-layer model by ignoring the intra-bilayer coupling J_c. Figure 8(a) shows the calculated data for various J_2/J_1 by taking $J_1 = 30.7$ K plotted with the experimental data. The MC data showed that as J_2/J_1 decreased, the peak value of χ was almost unchanged, while the peak temperature increased. The comparison with the experimental data, however, was not satisfactory, even at $J_2/J_1 = 0.12$. Therefore, in the absence of J_c, J_2/J_1 was expected to be smaller than the critical value of 0.15, below which the ground state exhibits a long-range order.

Next, we introduced J_c, since the crystal had a bilayer structure and the neutron diffraction suggested the presence of J_c.[12] The calculated data showed that as J_c/J_1 increased

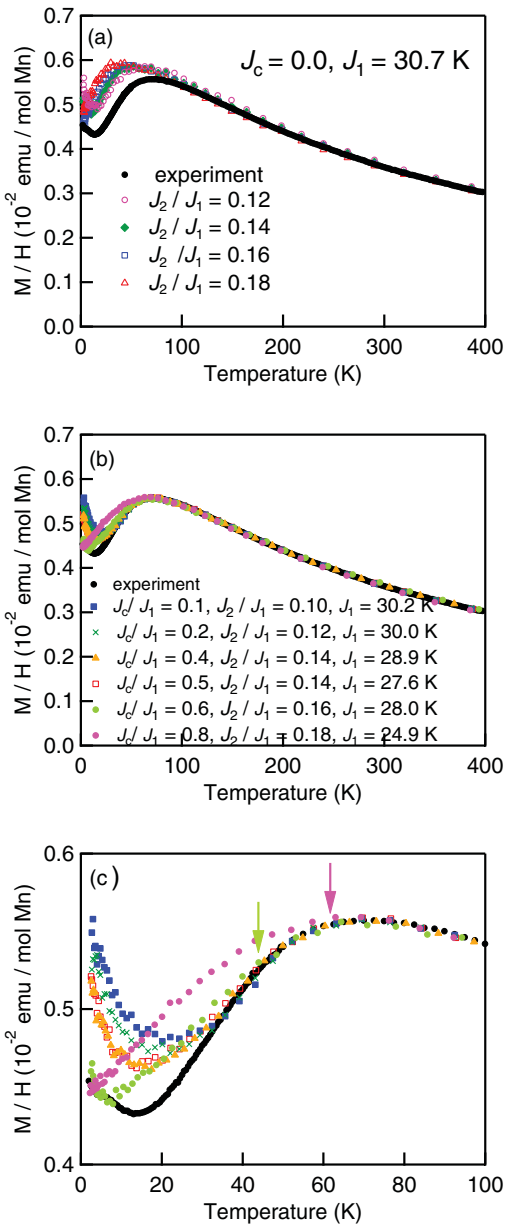

FIG. 8. (Color online) Comparison of the calculated and the experimental susceptibility of $Bi_3Mn_4O_{12}(NO_3)$. (a) J_2/J_1 dependence with $J_1 = 30.7$ K and $J_c/J_1 = 0.0$ and (b) the results assuming various combinations of J_2/J_1, J_c/J_1, and J_1. (c) Magnified view of (b).

for a fixed J_2/J_1, the peak temperature of χ increased, and the peak value decreased. We compared the results with the experimental data for the values of J_2/J_1 ranging from 0.10 to 0.18 by choosing an appropriate value of J_c/J_1 for each J_2/J_1 to fit the data above the peak. As shown in Fig. 8(b), J_c improved the fitting; the calculation reproduced the experimental data in a temperature range wider than that in Fig. 8(a). The small discrepancy at low temperatures was presumably due to the system size effect. Despite the overall agreement, unfortunately, we could not determine a unique set of J_2/J_1 and J_c/J_1 from the comparison: A reasonable agreement was obtained by increasing both J_c/J_1 and J_2/J_1 in the range of parameters plotted in Fig. 8(b). However, J_c comparable to or larger than J_1, suggested by the first-principles calculation,[11] led to a substantial deviation from the experimental data. As shown in Fig. 8(c), the deviation temperature indicated by the arrow increased as J_c/J_1 became closer to 1.

It should be noted that the J_2/J_1 ratio did not exceed 0.15, even when $J_c/J_1 = 0.5$ was considered, i.e., the value suggested by neutron scattering.[12] Moreover, J_c is expected to increase the critical J_2/J_1 ratio because it stabilizes the long-range magnetic ordering. Hence, although the purely two-dimensional model does not show a true long-range order at finite temperatures, the results presented here strongly suggest that frustration solely by J_2 is insufficient to explain the absence of long-range order in this honeycomb system. To account for the disordered ground state, the introduction of other interactions might be necessary. The candidates are a ferromagnetic third-nearest-neighbor interaction to the opposite side of a hexagon mediated by the Mn-O-O-Mn bond J_3, as suggested by unrestricted Hartree-Fock calculations,[19] and a diagonal intra-bilayer interaction J_c' respectively shown in Figs. 1(a) and 1(b).

IV. SUMMARY

We investigated the magnetic ground state of frustrated $S = 3/2$ honeycomb lattice antiferromagnet $Bi_3Mn_4O_{12}(NO_3)$ and the magnitudes of the antiferromagnetic interactions. No long-range magnetic ordering was found by susceptibility, specific heat, and μSR measurements. Instead, spin glass–like freezing below 6 K was observed. A comparison with the results of a Monte Carlo simulation revealed the importance of intra-bilayer coupling and further neighbor interactions beyond those of second neighbors for explaining the absence of long-range magnetic ordering.

ACKNOWLEDGMENTS

This work was partially supported by Grants-in-Aid from the Ministry of Education, Culture, Sports, Science and Technology, Japan for Scientific Research (Nos. 19GS0207, 19340098, 19052008, and 22244044), the Joint Project of Chemical Synthesis Core Research Institutions, and the Cabinet Office of the Government of Japan through its "Funding Program for Next Generation World-Leading Researchers." The SXRD experiment was conducted by using the beamline BL02B2 at SPring-8 with the approval of JASRI.

*Corresponding author: mazuma@msl.titech.ac.jp

[1] A. P. Ramirez, Ann. Rev. Mater. Sci. **24**, 453 (1994).

[2] S. Nakatsuji, Y. Nambu, H. Tonomura, O. Sakai, S. Jonas, C. Broholm, H. Tsunetsugu, Y. M. Qiu, and Y. Maeno, Science **309**, 1697 (2005).

[3] M. P. Shores, E. A. Nytko, B. M. Bartlett, and D. G. Nocera, J. Am. Chem. Soc. **127**, 13462 (2005).

[4] A. P. Ramirez, G. P. Espinosa, and A. S. Cooper, Phys. Rev. Lett. **64**, 2070 (1990).

[5]M. Nishiyama, S. Maegawa, T. Inami, and Y. Oka, Phys. Rev. B **67**, 224435 (2003).
[6]S. Katsura, T. Ide, and T. Morita, J. Stat. Phys. **42**, 381 (1986).
[7]K. Takano, Phys. Rev. B **74**, 140402 (2006).
[8]O. Smirnova, M. Azuma, N. Kumada, Y. Kusano, M. Matsuda, Y. Shimakawa, T. Takei, Y. Yonesaki, and N. Kinomura, J. Am. Chem. Soc. **131**, 8313 (2009).
[9]S. Okumura, H. Kawamura, T. Okubo, and Y. Motome, J. Phys. Soc. Jpn. **79**, 114705 (2010).
[10]A. Mulder, R. Ganesh, L. Capriotti, and A. Paramekanti, Phys. Rev. B **81**, 214419 (2010).
[11]H. C. Kandpal and J. van den Brink, Phys. Rev. B **83**, 140412 (2011).
[12]M. Matsuda, M. Azuma, M. Tokunaga, Y. Shimakawa, and N. Kumada, Phys. Rev. Lett. **105**, 187201 (2010).
[13]R. Ganesh, D. N. Sheng, Y.-J. Kim, and A. Paramekanti, Phys. Rev. B **83**, 144414 (2011).
[14]A. Schenck, *Muon Spin Rotation Spectroscopy: Principles and Applications in Solid State Physics* (Hilger, Bristol, 1985).
[15]K. Hukushima and K. Nemoto, J. Phys. Soc. Jpn. **65**, 1604 (1996).
[16]R. Kadono, J. Imazato, T. Matsuzaki, K. Nishiyama, K. Nagamine, T. Yamazaki, D. Richter, and J. M. Welter, Phys. Rev. B **39**, 23 (1989).
[17]R. Kadono, R. F. Kiefl, E. J. Ansaldo, J. H. Brewer, M. Celio, S. R. Kreitzman, and G. M. Luke, Phys. Rev. Lett. **64**, 665 (1990).
[18]S. Okubo, F. Elmasry, W. Zhang, M. Fujisawa, T. Sakurai, H. Ohta, M. Azuma, O. Sumirnova, and N. Kumada, J. Phys.: Conf. Ser. **200**, 022042 (2010).
[19]H. Wadati, K. Kato, Y. Wakisaka, T. Sudayama, D. G. Hawthorn, T. Z. Regier, N. Onishi, M. Azuma, Y. Shimakawa, T. Mizokawa, A. Tanaka, and G. A. Sawatzky, e-print arXiv:1101.2847v1.